

Long-distance decay-less spin transport in indirect excitons in a van der Waals heterostructure

Zhiwen Zhou,¹ E. A. Szwed,¹ D. J. Choksy,¹ L. H. Fowler-Gerace,¹ and L. V. Butov¹

¹*Department of Physics, University of California at San Diego, La Jolla, CA 92093, USA*

In addition to its fundamental interest, the long-distance spin transport with suppressed spin losses is essential for spintronic devices. However, the spin relaxation caused by scattering of the particles carrying the spin, limits the spin transport. We explored spatially indirect excitons (IXs), also known as interlayer excitons, in van der Waals heterostructures (HS) composed of atomically thin layers of transition-metal dichalcogenides (TMD) as spin carries. TMD HS also offer coupling of spin and valley transport. We observed the long-distance spin transport with the decay distances exceeding $100\ \mu\text{m}$ and diverging so spin currents show no decay in the HS. With increasing IX density, we observed spin localization, then long-distance spin transport, and then reentrant spin localization, in agreement with the Bose-Hubbard theory prediction for superfluid and insulating phases in periodic potentials due to moiré superlattices. The suppression of scattering in exciton superfluid suppresses the spin relaxation and enables the long-distance spin transport. This mechanism of protection against the spin relaxation makes IXs a platform for the realization of long-distance decay-less spin transport.

PACS numbers:

The physics of spin transport include a number of fundamental phenomena, including, in particular, the current-induced spin orientation (the spin Hall effect) [1–4], the spin drift, diffusion and drag [5–7], the quantum spin Hall effect [8–10], and the persistent spin helix [11]. In addition to its fundamental interest, the long-distance spin transport with suppressed spin losses is essential for developing spintronic devices, which may offer advantages in dissipation, size, and speed over charge-based devices [12].

IXs in HS can enable the realization of the long-distance spin transfer. IXs are composed of electrons and holes confined in separated layers [13]. Due to the separation of electron and hole layers, the IX lifetimes can exceed the lifetimes of spatially direct excitons (DXs) by orders of magnitude. Due to their long lifetimes, IXs can cool down below the temperature of quantum degeneracy and form a condensate [14] and can travel over long distances [15]. Travelling particles can transfer the spin state. However, the particle scattering causes fluctuating effective magnetic fields originating from the spin-orbit interaction in noncentrosymmetric materials and, as a result, causes the spin relaxation that limits the spin transfer [16]. Therefore, the suppression of scattering in IX condensate can suppress the spin relaxation and allow the long-distance spin transport. In addition, the electron-hole separation in IXs reduces the overlap of the electron and hole wave functions suppressing the spin relaxation due to electron-hole exchange [17].

IXs can be created in various HS, in particular, in GaAs HS [18–22], in GaN HS [23], and in ZnO HS [24]. Since the temperature of quantum degeneracy, which can be achieved for excitons, scales proportionally to the exciton binding energy E_X [25], IXs with high E_X can form a platform for the realization of high-temperature long-distance spin transport.

IXs in GaAs HS have low $E_X \lesssim 10\ \text{meV}$ [26, 27] and the

highest $E_X \sim 30\ \text{meV}$ for IXs in III-V and II-VI semiconductor HS is achieved in ZnO HS [24]. TMD HS enable the realization of excitons with remarkably high binding energies [28–31] and E_X for IXs in TMD HS reach hundreds of meV [25, 32, 33].

TMD HS also give an opportunity to explore spin transport in periodic potentials due to moiré superlattices. The period of the latter $b \approx a/\sqrt{\delta\theta^2 + \delta^2}$ is typically in the 10 nm range (a is the lattice constant, δ the lattice mismatch, $\delta\theta$ the deviation of the twist angle between the layers from $i\pi/3$, i is an integer) [34–49]. The moiré potentials can be affected by atomic reconstruction [50–52] and by disorder. In addition, due to the coupling of the spin and valley indices in TMD HS [53–56], the spin transport is coupled to the valley transport (therefore, for simplicity, we will use the term ‘spin’ also for ‘spin-valley’).

Earlier studies led to the observation of spin transport with $1/e$ decay distances $d_{1/e}^s$ up to a few μm in IXs in TMD HS [57–60]. Spin transport on a μm scale was also observed in DXs [61] and the excitation-induced polarization was found to lead to the emergence of ferromagnetic order [62] and to electron or hole spin transport with the spin diffusion length up to ca. $20\ \mu\text{m}$ [63, 64] in TMD. Spin relaxation due to scattering of the particles carrying the spin limited spin transport distances [16].

In this work, we observed in IXs in a $\text{MoSe}_2/\text{WSe}_2$ HS the long-distance spin transport with $d_{1/e}^s$ exceeding $100\ \mu\text{m}$ and diverging so spin currents show no decay in the HS. With increasing IX density, we observed spin localization, then long-distance spin transport, and then reentrant spin localization, in agreement with the Bose-Hubbard theory prediction for superfluid and insulating phases in periodic potentials due to moiré superlattices [65]. The suppression of scattering in exciton superfluid suppresses the spin relaxation and enables the long-distance spin transport.

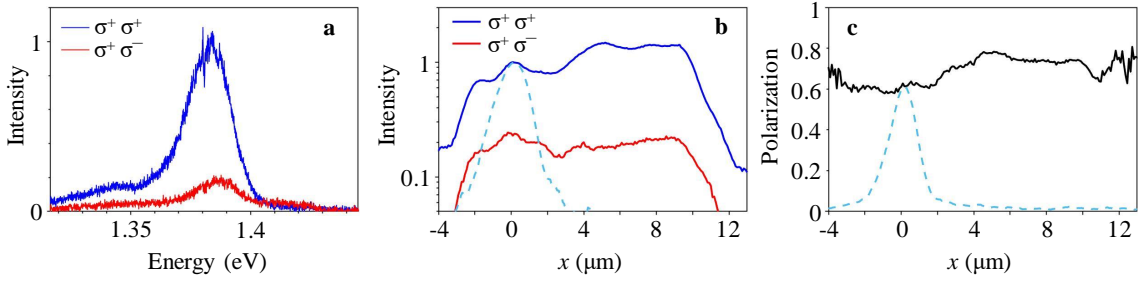


FIG. 1: The long-distance spin-valley polarization transport in IXs in MoSe₂/WSe₂ HS. (a) The circular polarization of IX PL. The blue (red) spectrum is co-polarized (cross-polarized) with the circularly polarized laser excitation. (b) Co-polarized I_{σ^+} (blue) and cross-polarized I_{σ^-} (red) IX PL intensity vs. the distance from the laser excitation spot centered at $x = 0$. The IX PL is spectrally integrated in the range $E < 1.4$ eV. The dashed line shows the DX PL profile in the MoSe₂ ML, this profile is close to the laser excitation profile for short-range DX transport. The HS active area extends from $x \sim -3$ to $10 \mu\text{m}$. The polarized IX PL propagates through the entire HS. (c) The degree of circular polarization of IX PL $P = (I_{\sigma^+} - I_{\sigma^-}) / (I_{\sigma^+} + I_{\sigma^-})$ vs. the transport distance. No decay is observed for the polarization transport for IXs over the entire HS. The laser excitation power $P_{\text{ex}} = 0.2$ mW, $T = 1.7$ K.

We study MoSe₂/WSe₂ HS assembled by stacking mechanically exfoliated 2D crystals [Fig. S1 in Supplementary Information (SI)]. IXs are formed from electrons and holes confined in adjacent MoSe₂ and WSe₂ monolayers (ML), respectively, encapsulated by hBN layers. No voltage is applied in the HS. IXs form the lowest-energy exciton state in the MoSe₂/WSe₂ HS (Fig. S1 in SI). The HS details are presented in SI.

Both the long-distance IX transport [66] and the long-distance spin transport, which is described below, are realized when the optical excitation has the energy E_{ex} close to the energy of DXs in the HS. The resonant excitation allows lowering the excitation-induced heating of the IX system. In particular, the colder IXs created by the resonant excitation screen the HS disorder more effectively that facilitates the emergence of IX superfluidity [67–69]. In this work, the laser excitation with $E_{\text{ex}} = 1.689$ eV is resonant to WSe₂ DX.

Both spin generation and detection in IXs is achieved by optical means via photon polarization. The circularly polarized laser excitation is focused to a $\sim 2 \mu\text{m}$ spot and the spin propagation is detected by the polarization-resolved PL imaging. Figure 1a shows a high degree of circular polarization in the excitation spot, indicating an effective relaxation of the optically generated spin-polarized DXs to the spin-polarized IXs with the spin relaxation time long compared to the exciton recombination and energy relaxation times.

The propagation of spin-polarized IXs from the excitation spot transfer the spin polarization. Remarkably, both the intensities of co-polarized and cross-polarized IX PL I_{σ^+} and I_{σ^-} (Fig. 1b) and the degree of circular polarization of IX PL $P = (I_{\sigma^+} - I_{\sigma^-}) / (I_{\sigma^+} + I_{\sigma^-})$ (Fig. 1c) propagate over the entire HS with no losses.

IX transport is characterized by the propagation of total IX intensity in both circular polarizations $n \sim I_{\sigma^+} + I_{\sigma^-}$. In turn, transport of spin polarization density carried

by IXs is characterized by the propagation of $I_{\text{spin}} = Pn = I_{\sigma^+} - I_{\sigma^-}$. The dependence of spin transport on excitation power P_{ex} and temperature is described below.

The spin transport nonmonotonically varies with increasing P_{ex} , increases at $P_{\text{ex}} \lesssim 0.2$ mW (Fig. 2a) and reduces at $P_{\text{ex}} \gtrsim 0.2$ mW (Fig. 2b), and vanishes at high temperatures (Fig. 2c). The spin transport is characterized by the $1/e$ decay distance of the spin polarization density $d_{1/e}^s$. The variation of spin transport with excitation power and temperature is presented by the variation of $d_{1/e}^s$ in Fig. 3.

For low P_{ex} , a single IX PL line is observed in the spectra. However, a higher-energy IX PL line appears in the spectrum at high P_{ex} (Fig. 4). We will refer to the IXs corresponding to these PL lines as the lower-energy IXs (LE-IXs) and higher-energy IXs (HE-IXs). Figures 2 and 3 present the spin transport carried by LE-IXs. $d_{1/e}^s$ (Fig. 3) are obtained from least-squares fitting the LE-IX spin density transport profiles $I_{\text{spin}}(x)$ (Fig. 2) to exponential decays in the HS. The HS dimensions allow establishing that the longest $d_{1/e}^s$ exceed $100 \mu\text{m}$. The data with the fit indicating diverging $d_{1/e}^s$, that is with no spin density decay within the entire HS, are presented by circles on the edge in Fig. 3a,b and by cyan color in Fig. 3c.

The data are discussed below. The spin transport (Fig. 3) is carried by LE-IXs and can be compared with the LE-IX transport (Fig. 4c and Fig. S7 in SI). Due to the separation d_z between the electron and hole layers, IXs have electric dipoles ed_z and the interaction between IXs is repulsive [70]. IXs in moiré superlattices form a system of repulsively interacting bosons in periodic potentials. The enhancement followed by the suppression of the LE-IX transport with density (Fig. 4c) is in qualitative agreement with the Bose-Hubbard theory of bosons in periodic potentials predicting superfluid at $N \sim 1/2$ and insulating at $N \sim 0$ and $N \sim 1$ phases [65]. For the maximum LE-IX transport distances observed

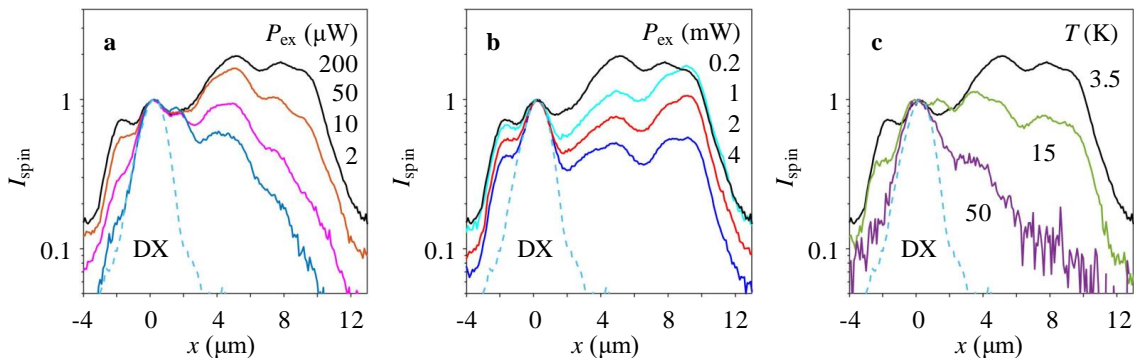


FIG. 2: Excitation power and temperature dependence of spin transport in LE-IXs. (a-c) Normalized spin density profiles $I_{\text{spin}} = Pn = I_{\sigma^+} - I_{\sigma^-}$ for the LE-IXs for different P_{ex} (a,b) and temperatures (c). The dashed line shows the DX luminescence profile in the MoSe₂ ML, this profile is close to the laser excitation profile for short-range DX transport. The LE-IX spectra are separated from the HE-IX spectra by the spectral integration in the range $E < 1.4$ eV. The HE-IXs appear in the spectra at high $P_{\text{ex}} \gtrsim 0.2$ mW (Fig. 4). The ~ 2 μm laser spot is centered at $x = 0$ (a-c), $T = 3.5$ K (a,b), $P_{\text{ex}} = 0.2$ mW (c).

at $P_{\text{ex}} \sim 0.2$ mW (Fig. 4c), the LE-IX density n estimated from the energy shift δE as $n = \delta E \varepsilon / 4\pi e^2 d_z$ [70] is $n \sim 2 \times 10^{11} \text{ cm}^{-2}$ ($d_z \sim 0.6$ nm, the dielectric constant $\varepsilon \sim 7.4$ [71]). This density is well below the Mott transition density $n_{\text{Mott}} > 10^{12} \text{ cm}^{-2}$ [25, 72]. $N \sim 1/2$ at $n \sim 2 \times 10^{11} \text{ cm}^{-2}$ for the moiré superlattice period $b = 17$ nm. This period $b \sim a/\delta\theta$ corresponds to the twist angle $\delta\theta = 1.1^\circ$, which agrees with the angle between MoSe₂ and WSe₂ edges in the HS (Fig. S1 in SI). This rough estimate indicates that the observation of LE-IX localization, then long-range transport, and then localization with increasing density (Fig. 4c) is in agreement with the Bose-Hubbard theory [65]. The density dependence of spin transport (Fig. 3a) is qualitatively similar to the density dependence of LE-IX transport (Fig. 4c).

Furthermore, the temperature dependence of spin transport is qualitatively similar to the temperature dependence of LE-IX transport: Both the long-distance spin transport (Fig. 3) and the long-distance LE-IX transport (Fig. S7 in SI) vanish at $T \sim 10$ K.

The similarity of the parameter dependence of the spin transport and the IX transport indicates that the dominant mechanism of the decay of spin density is the decay of IX density. The suppression of IX scattering, which leads to the long-distance IX transport (Fig. S7 in SI), also leads to the long-distance spin transport with $d_{1/e}^s$ exceeding 100 μm and diverging so spin currents show no decay in the HS (Fig. 3). This is consistent with the theory prediction that the suppression of scattering can cause the suppression of spin relaxation [16].

This indicates that the long-distance spin transport with suppressed losses can be achieved at higher temperatures in IX systems with higher superfluidity temperatures T_c . The theory predicts that the superfluidity temperature for bosons in periodic potentials $T_c \sim 4\pi NJ$ and higher T_c can be achieved in lattices with higher inter-site

hopping J [73]. Higher J can be achieved in moiré superlattices with smaller periods in HS with larger twist angles $\delta\theta$, or in moiré superlattices with smaller amplitudes that can be realized in HS with the same-TMD electron and hole layers [74, 75], or by lowering the moiré superlattice amplitude by voltage [37, 76], or by adding a spacer (hBN) layer between the electron and hole layers [58]. For TMD HS with suppressed moiré potentials, the theory predicts high- T_c superfluidity [25, 33]. This, in turn, can enable the realization of high-temperature long-distance spin transport with suppressed losses.

The above data outline the long-distance spin transport carried by LE-IXs. Figure 4 shows that HE-IX PL appears in the spectrum at high P_{ex} . In contrast to the LE-IX PL, which is co-polarized, the HE-IX PL is cross-polarized with the circularly polarized laser excitation. A similar higher-energy IX PL was observed in earlier studies. Various interpretations for multiple IX PL lines were considered, including the excitonic states split due to the conduction band K-valley spin splitting [77], trions [78], excitonic states indirect in momentum space and split due to the valley energy difference [79, 80] or spin-orbit coupling [81], and excitonic states in moiré superlattice [40–46]. The data in Fig. 4 agree with the latter and indicate that the HE-IX PL corresponds to two IXs per moiré cell. The appearance of HE-IX PL in the spectrum (Fig. 4a,b) correlates with the onset of IX transport suppression (Fig. 4c). For the IX transport suppression caused by the high occupation of moiré cells, outlined above, this correlation indicates that the onset of HE-IX PL corresponds to the appearance of moiré cells with two IXs per cell. For moiré cells with two IXs, the IXs can emit in different polarizations [37], and the intra-cell IX repulsion enhances the IX energy [82, 83].

In summary, we observed in IXs in a MoSe₂/WSe₂ HS the long-distance spin transport with $1/e$ decay distances

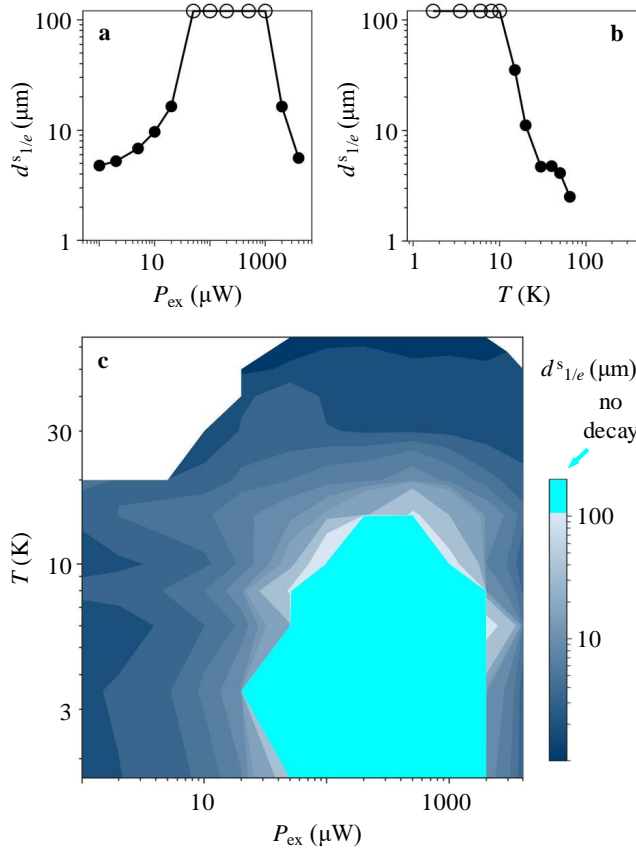


FIG. 3: Excitation power and temperature dependence of spin transport in LE-IXs. (a-c) The $1/e$ decay distance $d_{1/e}^s$ of spin density transport $I_{\text{spin}} = Pn = I_{\sigma^+} - I_{\sigma^-}$ in LE-IXs vs. P_{ex} (a), vs. temperature (b), and vs. P_{ex} and temperature (c). $d_{1/e}^s$ are obtained from least-squares fitting the LE-IX spin density transport profiles $I_{\text{spin}}(x)$ (Fig. 2) to exponential decays in the region $x = 0 - 9 \mu\text{m}$. The data with the fit indicating diverging $d_{1/e}^s$ are presented by circles on the edge (a,b) or by cyan color (c). The LE-IX spectra are separated from the HE-IX spectra by the gaussian fits. The HE-IXs appear in the spectra at high $P_{\text{ex}} \gtrsim 0.2 \text{ mW}$ (Fig. 4). $T = 3.5 \text{ K}$ (a), $P_{\text{ex}} = 0.2 \text{ mW}$ (b).

exceeding $100 \mu\text{m}$ and diverging so spin currents show no decay in the HS. With increasing IX density, we observed spin localization, then long-distance spin transport, and then reentrant spin localization, in agreement with the Bose-Hubbard theory prediction for superfluid and insulating phases in periodic potentials due to moiré superlattices. The suppression of scattering in exciton superfluid suppresses the spin relaxation and enables the long-distance spin transport.

We thank M.M. Fogler and J.R. Leonard for discussions. We especially thank A.H. MacDonald for discussions of IXs in moiré potentials and A.K. Geim for teaching us manufacturing TMD HS. The studies were supported by DOE Office of Basic Energy Sciences under Award DE-FG02-07ER46449. The HS manufacturing

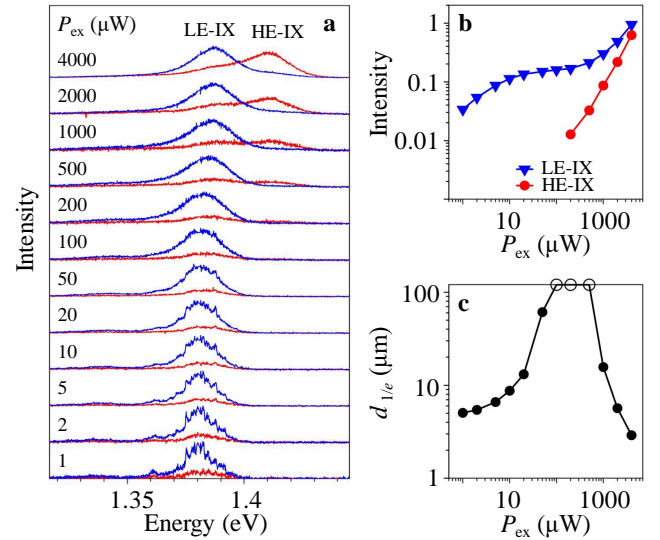


FIG. 4: Density dependence of IX PL spectra. (a) The excitation power dependence of co-polarized (blue) and cross-polarized (red) IX spectra. The LE-IX PL is co-polarized. The HE-IX PL is cross-polarized. The HE-IXs appear in the spectra at high $P_{\text{ex}} \gtrsim 0.2 \text{ mW}$. The spectral profile separation of LE-IXs and HE-IXs is presented in Fig. S3 in SI. (b) The intensity of LE-IX PL (blue triangles) and HE-IX PL (red points) vs. P_{ex} . (c) The $1/e$ LE-IX transport decay distance $d_{1/e}$ vs. P_{ex} . $d_{1/e}$ are obtained from least-squares fitting the spectrally integrated LE-IX PL intensity including both polarizations $I_{\sigma^+} + I_{\sigma^-}$ to exponential decays in the region $x = 0 - 9 \mu\text{m}$. $T = 3.5 \text{ K}$.

was supported by NSF Grant 1905478.

- [1] M.I. D'yakonov, V.I. Perel', Current-induced spin orientation of electrons in semiconductors. *Phys. Lett. A* **35**, 459 (1971).
- [2] J.E. Hirsch, Spin Hall Effect. *Phys. Rev. Lett.* **83**, 1834 (1999).
- [3] Jairo Sinova, Dimitrie Culcer, Q. Niu, N.A. Sinitsyn, T. Jungwirth, A.H. MacDonald, Universal Intrinsic Spin Hall Effect. *Phys. Rev. Lett.* **92**, 126603 (2004).
- [4] Y.K. Kato, R.C. Myers, A.C. Gossard, D.D. Awschalom, Observation of the Spin Hall Effect in Semiconductors. *Science* **306**, 1910 (2004).
- [5] J.M. Kikkawa, D.D. Awschalom, Lateral drag of spin coherence in gallium arsenide. *Nature* **397**, 139 (1999).
- [6] C.P. Weber, N. Gedik, J.E. Moore, J. Orenstein, J. Stephens, D.D. Awschalom, Observation of spin Coulomb drag in a two-dimensional electron gas. *Nature* **437**, 1330 (2005).
- [7] S.A. Crooker, M. Furis, X. Lou, C. Adelman, D.L. Smith, C.J. Palmström, P.A. Crowell, Imaging Spin Transport in Lateral Ferromagnet/Semiconductor Structures. *Science* **309**, 2191 (2005).
- [8] C.L. Kane, E.J. Mele, Z_2 Topological Order and the Quantum Spin Hall Effect. *Phys. Rev. Lett.* **95**, 146802 (2005).
- [9] B. Andrei Bernevig, Shou-Cheng Zhang, Quantum Spin Hall Effect. *Phys. Rev. Lett.* **96**, 106802 (2006).
- [10] Markus König, Steffen Wiedmann, Christoph Brüne, An-

- deas Roth, Hartmut Buhmann, Laurens W. Molenkamp, Xiao-Liang Qi, Shou-Cheng Zhan, Quantum Spin Hall Insulator State in HgTe Quantum Wells. *Science* **318**, 766 (2007).
- [11] J.D. Koralek, C.P. Weber, J. Orenstein, B.A. Bernevig, Shou-Cheng Zhang, S. Mack, D.D. Awschalom, Emergence of the persistent spin helix in semiconductor quantum wells. *Nature* **458**, 610 (2009).
- [12] D.D. Awschalom, M.E. Flatté, Challenges for semiconductor spintronics. *Nat. Phys.* **3**, 153 (2007).
- [13] Y.E. Lozovik, V.I. Yudson, A new mechanism for superconductivity: pairing between spatially separated electrons and holes. *Sov. Phys. JETP* **44**, 389 (1976).
- [14] A.A. High, J.R. Leonard, A.T. Hammack, M.M. Fogler, L.V. Butov, A.V. Kavokin, K.L. Campman, A.C. Gossard, Spontaneous coherence in a cold exciton gas. *Nature* **483**, 584 (2012).
- [15] M. Hagn, A. Zrenner, G. Böhm, G. Weimann, Electric-field-induced exciton transport in coupled quantum well structures. *Appl. Phys. Lett.* **67**, 232 (1995).
- [16] M.I. Dyakonov, *Spin Physics in Semiconductors* (Springer, New York, 2008).
- [17] M.Z. Maialle, E.A. de Andrada e Silva, L.J. Sham, Exciton spin dynamics in quantum wells. *Phys. Rev. B* **47**, 15776 (1993).
- [18] J.R. Leonard, Y.Y. Kuznetsova, Sen Yang, L.V. Butov, T. Ostatnický, A. Kavokin, A.C. Gossard, Spin Transport of Excitons. *Nano Lett.* **9**, 4204 (2009).
- [19] A.A. High, A.T. Hammack, J.R. Leonard, Sen Yang, L.V. Butov, T. Ostatnický, M. Vladimirova, A.V. Kavokin, T.C.H. Liew, K.L. Campman, A.C. Gossard, Spin Currents in a Coherent Exciton Gas. *Phys. Rev. Lett.* **110**, 246403 (2013).
- [20] A. Violante, R. Hey, P.V. Santos, Coherent transport and manipulation of spins in indirect-exciton nanostructures. *Phys. Rev. B* **91**, 125302 (2015).
- [21] R. Finkelstein, K. Cohen, B. Jouault, K. West, L.N. Pfeiffer, M. Vladimirova, R. Rapaport, Transition from spin-orbit to hyperfine interaction dominated spin relaxation in a cold fluid of dipolar excitons. *Phys. Rev. B* **96**, 085404 (2017).
- [22] J.R. Leonard, A.A. High, A.T. Hammack, M.M. Fogler, L.V. Butov, K.L. Campman, A.C. Gossard, Pancharatnam-Berry phase in condensate of indirect excitons. *Nat. Commun.* **9**, 2158 (2018).
- [23] François Chiaruttini, Thierry Guillet, Christelle Brimont, Benoit Jouault, Pierre Lefebvre, Jessica Vives, Sebastien Chenot, Yvon Cordier, Benjamin Damilano, Maria Vladimirova, Trapping Dipolar Exciton Fluids in GaN/(AlGa)N Nanostructures. *Nano Lett.* **19**, 4911 (2019).
- [24] C. Morhain, T. Bretagnon, P. Lefebvre, X. Tang, P. Valvin, T. Guillet, B. Gil, T. Taliercio, M. Teisseire-Doninelli, B. Vinter, C. Deparis, Internal electric field in wurtzite ZnO/Zn_{0.78}Mg_{0.22}O quantum wells. *Phys. Rev. B* **72**, 241305(R) (2005).
- [25] M.M. Fogler, L.V. Butov, K.S. Novoselov, High-temperature superfluidity with indirect excitons in van der Waals heterostructures. *Nat. Commun.* **5**, 4555 (2014).
- [26] A. Zrenner, P. Leeb, J. Schäfler, G. Böhm, G. Weimann, J.M. Worlock, L.T. Florez, J.P. Harbison, Indirect excitons in coupled quantum well structures. *Surf. Sci.* **263**, 496 (1992).
- [27] K. Sivalertporn, L. Mouchliadis, A.L. Ivanov, R. Philp, E.A. Muljarov, Direct and indirect excitons in semiconductor coupled quantum wells in an applied electric field. *Phys. Rev. B* **85**, 045207 (2012).
- [28] A.K. Geim, I.V. Grigorieva, Van der Waals heterostructures. *Nature* **499**, 419 (2013).
- [29] Ziliang Ye, Ting Cao, Kevin O'Brien, Hanyu Zhu, Xiaobo Yin, Yuan Wang, Steven G. Louie, Xiang Zhang, Probing excitonic dark states in single-layer tungsten disulphide. *Nature* **513**, 214 (2014).
- [30] Alexey Chernikov, Timothy C. Berkelbach, Heather M. Hill, Albert Rigosi, Yilei Li, Ozgur Burak Aslan, David R. Reichman, Mark S. Hybertsen, Tony F. Heinz, Exciton Binding Energy and Nonhydrogenic Rydberg Series in Monolayer WS₂. *Phys. Rev. Lett.* **113**, 076802 (2014).
- [31] M. Goryca, J. Li, A.V. Stier, T. Taniguchi, K. Watanabe, E. Courtade, S. Shree, C. Robert, B. Urbaszek, X. Marie, S.A. Crooker, Revealing exciton masses and dielectric properties of monolayer semiconductors with high magnetic fields. *Nat. Commun.* **10**, 4172 (2019).
- [32] Thorsten Deilmann, Kristian Sommer Thygesen, Interlayer Trions in the MoS₂/WS₂ van der Waals Heterostructure. *Nano Lett.* **18**, 1460 (2018).
- [33] Oleg L. Berman, Roman Ya. Kezerashvili, Superfluidity of dipolar excitons in a transition metal dichalcogenide double layer. *Phys. Rev. B* **96**, 094502 (2017).
- [34] Fengcheng Wu, Timothy Lovorn, A.H. MacDonald, Theory of optical absorption by interlayer excitons in transition metal dichalcogenide heterobilayers. *Phys. Rev. B* **97**, 035306 (2018).
- [35] Hongyi Yu, Gui-Bin Liu, Wang Yao, Brightened spin-triplet interlayer excitons and optical selection rules in van der Waals heterobilayers. *2D Mater.* **5**, 035021 (2018).
- [36] Fengcheng Wu, Timothy Lovorn, A.H. MacDonald, Topological Exciton Bands in Moiré Heterojunctions. *Phys. Rev. Lett.* **118**, 147401 (2017).
- [37] Hongyi Yu, Gui-Bin Liu, Jianju Tang, Xiaodong Xu, Wang Yao, Moiré excitons: From programmable quantum emitter arrays to spin-orbit-coupled artificial lattices. *Sci. Adv.* **3**, e1701696 (2017).
- [38] Chendong Zhang, Chih-Piao Chuu, Xibiao Ren, Ming-Yang Li, Lain-Jong Li, Chuanhong Jin, Mei-Yin Chou, Chih-Kang Shih, Interlayer couplings, Moiré patterns, and 2D electronic superlattices in MoS₂/WSe₂ hetero-bilayers. *Sci. Adv.* **3**, e1601459 (2017).
- [39] Pasqual Rivera, Hongyi Yu, Kyle L. Seyler, Nathan P. Wilson, Wang Yao, Xiaodong Xu, Interlayer valley excitons in heterobilayers of transition metal dichalcogenides. *Nat. Nanotechnol.* **13**, 1004 (2018).
- [40] Nan Zhang, Alessandro Surrente, Michał Baranowski, Duncan K. Maude, Patricia Gant, Andres Castellanos-Gomez, Paulina Plochocka, Moiré Intralayer Excitons in a MoSe₂/MoS₂ Heterostructure. *Nano Lett.* **18**, 7651 (2018).
- [41] Alberto Ciarrocchi, Dmitrii Unuchek, Ahmet Avsar, Kenji Watanabe, Takashi Taniguchi, Andras Kis, Polarization switching and electrical control of interlayer excitons in two-dimensional van der Waals heterostructures. *Nat. Photonics* **13**, 131 (2019).
- [42] Kyle L. Seyler, Pasqual Rivera, Hongyi Yu, Nathan P. Wilson, Essance L. Ray, David G. Mandrus, Jiaqiang Yan, Wang Yao, Xiaodong Xu, Signatures of moiré-trapped valley excitons in MoSe₂/WSe₂ heterobilayers. *Nature* **567**, 66 (2019).
- [43] Kha Tran, Galan Moody, Fengcheng Wu, Xiaobo Lu, Junho Choi, Kyoungwan Kim, Amrithesh Rai, Daniel A. Sanchez, Jiamin Quan, Akshay Singh, Jacob Embley,

- André Zepeda, Marshall Campbell, Travis Autry, Takashi Taniguchi, Kenji Watanabe, Nanshu Lu, Sanjay K. Banerjee, Kevin L. Silverman, Suenne Kim, Emanuel Tutuc, Li Yang, Allan H. MacDonald, Xiaoqin Li, Evidence for moiré excitons in van der Waals heterostructures. *Nature* **567**, 71 (2019).
- [44] Chenhao Jin, Emma C. Regan, Aiming Yan, M. Iqbal Bakti Utama, Danqing Wang, Sihan Zhao, Ying Qin, Sijie Yang, Zhiren Zheng, Shenyang Shi, Kenji Watanabe, Takashi Taniguchi, Sefaattin Tongay, Alex Zettl, Feng Wang, Observation of moiré excitons in WSe_2/WS_2 heterostructure superlattices. *Nature* **567**, 76 (2019).
- [45] Evgeny M. Alexeev, David A. Ruiz-Tijerina, Mark Danovich, Matthew J. Hamer, Daniel J. Terry, Pramoda K. Nayak, Seongjoon Ahn, Sangyeon Pak, Juwon Lee, Jung Inn Sohn, Maciej R. Molas, Maciej Koperski, Kenji Watanabe, Takashi Taniguchi, Kostya S. Novoselov, Roman V. Gorbachev, Hyeon Suk Shin, Vladimir I. Fal'ko, Alexander I. Tartakovskii, Resonantly hybridized excitons in moiré superlattices in van der Waals heterostructures. *Nature* **567**, 81 (2019).
- [46] Chenhao Jin, Emma C. Regan, Danqing Wang, M. Iqbal Bakti Utama, Chan-Shan Yang, Jeffrey Cain, Ying Qin, Yuxia Shen, Zhiren Zheng, Kenji Watanabe, Takashi Taniguchi, Sefaattin Tongay, Alex Zettl, Feng Wang, Identification of spin, valley and moiré quasi-angular momentum of interlayer excitons. *Nat. Phys.* **15**, 1140 (2019).
- [47] Yuya Shimazaki, Ido Schwartz, Kenji Watanabe, Takashi Taniguchi, Martin Kroner, Ataç Imamoğlu, Strongly correlated electrons and hybrid excitons in a moiré heterostructure. *Nature* **580**, 472 (2020).
- [48] Nathan P. Wilson, Wang Yao, Jie Shan, Xiaodong Xu, Excitons and emergent quantum phenomena in stacked 2D semiconductors. *Nature* **599**, 383 (2021).
- [49] Jie Gu, Liguang Ma, Song Liu, Kenji Watanabe, Takashi Taniguchi, James C. Hone, Jie Shan, Kin Fai Mak, Dipolar excitonic insulator in a moiré lattice. *Nat. Phys.* **18**, 395 (2022).
- [50] Astrid Weston, Yichao Zou, Vladimir Enaldiev, Alex Summerfield, Nicholas Clark, Viktor Zólyomi, Abigail Graham, Celal Yelgel, Samuel Magorrian, Mingwei Zhou, Johanna Zultak, David Hopkinson, Alexei Barinov, Thomas H. Bointon, Andrey Kretinin, Neil R. Wilson, Peter H. Beton, Vladimir I. Fal'ko, Sarah J. Haigh, Roman Gorbachev, Atomic reconstruction in twisted bilayers of transition metal dichalcogenides. *Nat. Nanotechnol.* **15**, 592 (2020).
- [51] Matthew R. Rosenberger, Hsun-Jen Chuang, Madeleine Phillips, Vladimir P. Oleshko, Kathleen M. McCreary, Saujan V. Sivaram, C. Stephen Hellberg, Berend T. Jonker, Twist Angle-Dependent Atomic Reconstruction and Moiré Patterns in Transition Metal Dichalcogenide Heterostructures. *ACS Nano* **14**, 4550 (2020).
- [52] Shen Zhao, Zhijie Li, Xin Huang, Anna Rupp, Jonas Göser, Ilia A. Vovk, Stanislav Yu. Kruchinin, Kenji Watanabe, Takashi Taniguchi, Ismail Bilgin, Anvar S. Baimuratov, Alexander Högele, Excitons in mesoscopically reconstructed moiré heterostructures. *Nat. Nanotechnol.* **18**, 572 (2023).
- [53] Di Xiao, Gui-Bin Liu, Wanxiang Feng, Xiaodong Xu, Wang Yao, Coupled Spin and Valley Physics in Monolayers of MoS_2 and Other Group-VI Dichalcogenides. *Phys. Rev. Lett.* **108**, 196802 (2012).
- [54] Ting Cao, Gang Wang, Wenpeng Han, Huiqi Ye, Chuanrui Zhu, Junren Shi, Qian Niu, Pingheng Tan, Enge Wang, Baoli Liu, Ji Feng, Valley-selective circular dichroism of monolayer molybdenum disulphide. *Nat. Commun.* **3**, 887 (2012).
- [55] Hualing Zeng, Junfeng Dai, Wang Yao, Di Xiao, Xiaodong Cui, Valley polarization in MoS_2 monolayers by optical pumping. *Nat. Nanotechnol.* **7**, 490 (2012).
- [56] Kin Fai Mak, Keliang He, Jie Shan, Tony F. Heinz, Control of valley polarization in monolayer MoS_2 by optical helicity. *Nat. Nanotechnol.* **7**, 494 (2012).
- [57] Pasqual Rivera, Kyle L. Seyler, Hongyi Yu, John R. Schaibley, Jiaqiang Yan, David G. Mandrus, Wang Yao, Xiaodong Xu, Valley-polarized exciton dynamics in a 2D semiconductor heterostructure. *Science* **351**, 688 (2016).
- [58] Dmitrii Unuchek, Alberto Ciarrocchi, Ahmet Avsar, Zhe Sun, Kenji Watanabe, Takashi Taniguchi, Andras Kis, Valley-polarized exciton currents in a van der Waals heterostructure. *Nat. Nanotechnol.* **14**, 1104 (2019).
- [59] Zumeng Huang, Yuanda Liu, Kevin Dini, Qinghai Tan, Zhuojun Liu, Hanlin Fang, Jin Liu, Timothy Liew, Weibo Gao, Robust Room Temperature Valley Hall Effect of Interlayer Excitons. *Nano Lett.* **20**, 1345 (2020).
- [60] Daniel N. Shanks, Fateme MahdikhanySarvejahany, Trevor G. Stanfill, Michael R. Koehler, David G. Mandrus, Takashi Taniguchi, Kenji Watanabe, Brian J. LeRoy, John R. Schaibley, Interlayer Exciton Diode and Transistor. *Nano Lett.* **22**, 6599 (2022).
- [61] Masaru Onga, Yijin Zhang, Toshiya Ideue, Yoshihiro Iwasa, Exciton Hall effect in monolayer MoS_2 . *Nat. Mater.* **16**, 1193 (2017).
- [62] Kai Hao, Robert Shreiner, Andrew Kindseth, Alexander A. High, Optically controllable magnetism in atomically thin semiconductors. *Sci. Adv.* **8**, eabq7650 (2022).
- [63] Chenhao Jin, Jonghwan Kim, M. Iqbal Bakti Utama, Emma C. Regan, Hans Kleemann, Hui Cai, Yuxia Shen, Matthew James Shinner, Arjun Sengupta, Kenji Watanabe, Takashi Taniguchi, Sefaattin Tongay, Alex Zettl, Feng Wang, Imaging of pure spin-valley diffusion current in WS_2 - WSe_2 heterostructures. *Science* **360**, 893 (2018).
- [64] L. Ren, L. Lombez, C. Robert, D. Beret, D. Lagarde, B. Urbaszek, P. Renucci, T. Taniguchi, K. Watanabe, S.A. Crooker, X. Marie, Optical Detection of Long Electron Spin Transport Lengths in a Monolayer Semiconductor. *Phys. Rev. Lett.* **129**, 027402 (2022).
- [65] Matthew P. A. Fisher, Peter B. Weichman, G. Grinstein, Daniel S. Fisher, Boson localization and the superfluid-insulator transition. *Phys. Rev. B* **40**, 546 (1989).
- [66] L.H. Fowler-Gerace, Zhiwen Zhou, E.A. Szwed, D.J. Choksy, L.V. Butov, Transport and localization of indirect excitons in a van der Waals heterostructure. arXiv:2307.00702 (2023).
- [67] Dmitri E. Nikonov, Ataç Imamoğlu, Bose condensation in two dimensions with disorder: Gross-Pitaevskii approach. arXiv:quant-ph/9806003 (1998).
- [68] A.L. Ivanov, L.E. Smallwood, A.T. Hammack, Sen Yang, L.V. Butov, A.C. Gossard, Origin of the inner ring in photoluminescence patterns of quantum well excitons. *Europhys. Lett.* **73**, 920 (2006).
- [69] M. Remeika, J.C. Graves, A.T. Hammack, A.D. Meyert-holen, M.M. Fogler, L.V. Butov, M. Hanson and A.C. Gossard, Localization-Delocalization Transition of Indirect Excitons in Lateral Electrostatic Lattices. *Phys. Rev. Lett.* **102**, 186803 (2009).
- [70] D. Yoshioka, A.H. MacDonald, Double quantum well electron-hole systems in strong magnetic fields. *J. Phys.*

- Soc. Jpn.* **59**, 4211 (1990).
- [71] Akash Laturia, Maarten L. Van de Put, William G. Vandenberghe, Dielectric properties of hexagonal boron nitride and transition metal dichalcogenides: from monolayer to bulk. *NPJ 2D Mater. Appl.* **2**, 6 (2018).
- [72] Jue Wang, Jenny Ardelean, Yusong Bai, Alexander Steinhoff, Matthias Florian, Frank Jahnke, Xiaodong Xu, Mackillo Kira, James Hone, X.-Y. Zhu, Optical generation of high carrier densities in 2D semiconductor heterobilayers. *Sci. Adv.* **5**, eaax0145 (2019).
- [73] Barbara Capogrosso-Sansone, Şebnem Güneş Söyler, Nikolay Prokof'ev, Boris Svistunov, Monte Carlo study of the two-dimensional Bose-Hubbard model. *Phys. Rev. A* **77**, 015602 (2008).
- [74] Zefang Wang, Yi-Hsin Chiu, Kevin Honz, Kin Fai Mak, Jie Shan, Electrical Tuning of Interlayer Exciton Gases in WSe₂ Bilayers. *Nano Lett.* **18**, 137 (2018).
- [75] E.V. Calman, M.M. Fogler, L.V. Butov, S. Hu, A. Mishchenko, A.K. Geim, Indirect excitons in van der Waals heterostructures at room temperature. *Nat. Commun.* **9**, 1895 (2018).
- [76] L.H. Fowler-Gerace, D.J. Choksy, L.V. Butov, Voltage-controlled long-range propagation of indirect excitons in a van der Waals heterostructure. *Phys. Rev. B* **104**, 165302 (2021).
- [77] Pasqual Rivera, John R. Schaibley, Aaron M. Jones, Jason S. Ross, Sanfeng Wu, Grant Aivazian, Philip Klement, Kyle Seyler, Genevieve Clark, Nirmal J. Ghimire, Jiaqiang Yan, D.G. Mandrus, Wang Yao, Xiaodong Xu, Observation of long-lived interlayer excitons in monolayer MoSe₂-WSe₂ heterostructures. *Nat. Commun.* **6**, 6242 (2015).
- [78] E.V. Calman, L.H. Fowler-Gerace, D.J. Choksy, L.V. Butov, D.E. Nikonov, I.A. Young, S. Hu, A. Mishchenko, A.K. Geim, Indirect Excitons and Trions in MoSe₂/WSe₂ van der Waals Heterostructures. *Nano Lett.* **20**, 1869 (2020).
- [79] Bastian Miller, Alexander Steinhoff, Borja Pano, Julian Klein, Frank Jahnke, Alexander Holleitner, Ursula Wurstbauer, Long-Lived Direct and Indirect Interlayer Excitons in van der Waals Heterostructures. *Nano Lett.* **17**, 5229 (2017).
- [80] Mitsuhiro Okada, Alex Kutana, Yusuke Kureishi, Yu Kobayashi, Yuika Saito, Tetsuki Saito, Kenji Watanabe, Takashi Taniguchi, Sunny Gupta, Yasumitsu Miyata, Boris I. Yakobson, Hisanori Shinohara, Ryo Kitaura, Direct and Indirect Interlayer Excitons in a van der Waals Heterostructure of hBN/WS₂/MoS₂/hBN. *ACS Nano* **12**, 2498 (2018).
- [81] Aubrey T. Hanbicki, Hsun-Jen Chuang, Matthew R. Rosenberger, C. Stephen Hellberg, Saujan V. Sivaram, Kathleen M. McCreary, Igor I. Mazin, Berend T. Jonker, Double Indirect Interlayer Exciton in a MoSe₂/WSe₂ van der Waals Heterostructure. *ACS Nano* **12**, 4719 (2018).
- [82] Spin transport in HE-IXs is shorter-range than in LE-IXs and is not considered in this work.
- [83] Narrow PL lines at low densities (Fig. 4a) can be related to localized states and are not considered in this work.

Supporting Information for Long-distance decay-less spin transport in indirect excitons in a van der Waals heterostructure

Zhiwen Zhou,¹ E. A. Szwed,¹ D. J. Choksy,¹ L. H. Fowler-Gerace,¹ and L. V. Butov¹

¹Department of Physics, University of California at San Diego, La Jolla, CA 92093, USA

PACS numbers:

The heterostructure details

The van der Waals MoSe₂/WSe₂ heterostructure (HS) was assembled using the dry-transfer peel-and-lift technique [1]. The same HS was used for the studies of IX transport in Ref. [2] and the HS manufacturing details are described in Ref. [2]. The thickness of bottom and top hBN layers is about 40 and 30 nm, respectively. The MoSe₂ monolayer is on top of the WSe₂ monolayer. The long WSe₂ and MoSe₂ edges reach ~ 30 and ~ 20 μm , respectively, which enables a rotational alignment between the WSe₂ and MoSe₂ monolayers. The twist angle $\delta\theta = 1.1^\circ$ corresponding to the moiré superlattice period $b = 17$ nm, which gives $N \sim 1/2$ at the estimated $n \sim 2 \times 10^{11}$ cm⁻² for the long-distance IX transport as outlined in the main text, agrees with the angle between MoSe₂ and WSe₂ edges in the HS (Fig. S1b).

The accuracies of estimating $\delta\theta$ using the long WSe₂ and MoSe₂ edges and using SHG are comparable. We do not use SHG for additional estimates of $\delta\theta$ since the intense optical excitation pulses in SHG measurements may cause a deterioration of the HS and may suppress both the long-distance IX transport and the long-distance spin transport. As outlined in the main text, the moiré potentials can be affected by atomic reconstruction and by disorder and may vary over the HS area.

Figure S1b presents a microscope image showing the layer pattern of the HS. The layer boundaries are indicated. The hBN layers cover the entire areas of MoSe₂ and WSe₂ layers. There was a narrow multilayer graphene electrode on the top of the HS around $x = 2$ μm for $y = 0$, Fig. S1b. This electrode was detached. The IX luminescence reduction around $x = 2$ μm can be related to residual graphene layers on the HS.

We did not verify if stacking in the sample is R or H (AA or AB). This is the subject for future works. We note however, that regardless the stacking type, the data in the paper demonstrate the proof-of-principle for the existence of long-distance spin transport in TMD HS. We note also that the characteristic energies in the IX system in the regime of the long-distance spin transport (Fig. 3), including the IX interaction energy $\delta E \sim 3$ meV and thermal energy $k_B T \lesssim 1$ meV (k_B is the Boltzmann constant), are considerably smaller than the estimated amplitudes of the moiré potential for both R and H stacking [3–6]. Besides the demonstration of the existence of long-distance spin

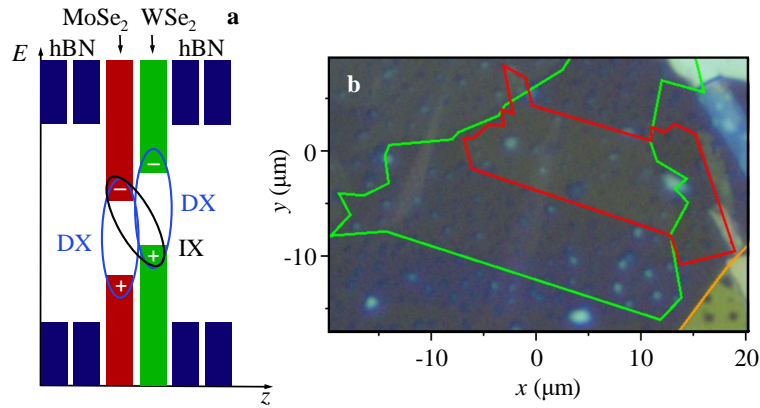


FIG. S1: (a) Schematic energy-band diagram for the MoSe₂/WSe₂ HS. The ovals indicate a direct exciton (DX) and an indirect exciton (IX) composed of an electron (-) and a hole (+). (b) A microscope image showing the layer pattern of the HS. The green and red lines indicate the boundaries of WSe₂ and MoSe₂ monolayers, respectively. The bottom and top hBN layers entirely cover the WSe₂ and MoSe₂ monolayers, the boundaries of bottom hBN layer are beyond the figure and a part of the boundaries of top hBN layer is shown by the orange line.

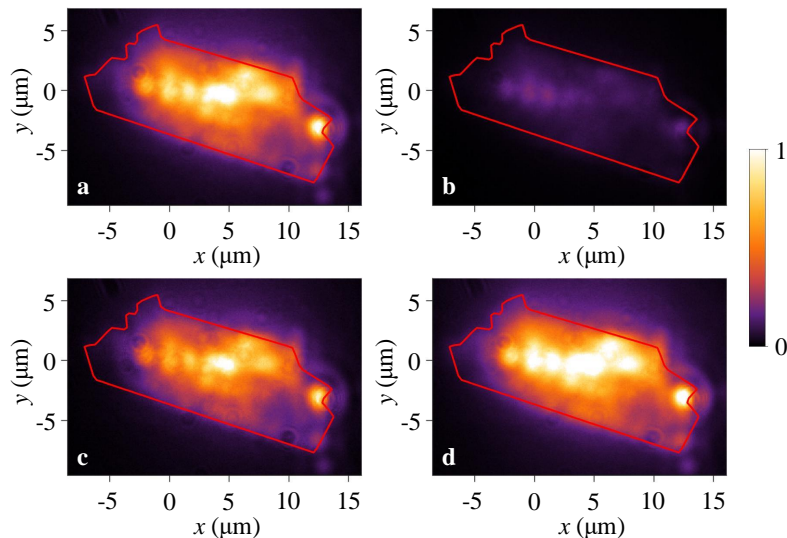


FIG. S2: (a,b) IX PL images co-polarized $I_{\sigma^+}(x, y)$ (a) and cross-polarized $I_{\sigma^-}(x, y)$ (b) with the circularly polarized laser excitation. The IX PL is selected by a filter $E \lesssim 1.4$ eV. (c) The spin density image $I_{\text{spin}} = Pn = I_{\sigma^+} - I_{\sigma^-}$. (d) The density image $n = I_{\sigma^+} + I_{\sigma^-}$. The $\sim 2 \mu\text{m}$ laser excitation spot is centered at $(0, 0)$, $P_{\text{ex}} = 0.2$ mW, $T = 1.7$ K.

transport in TMD HS, the studied $\text{MoSe}_2/\text{WSe}_2$ HS allows measuring the density-temperature phase diagram for this phenomenon and comparing it with the theory. However, it is essential to study this phenomenon in other samples and, in particular, to study the dependence on the twist angle. Both the long-distance IX transport and the long-distance spin transport require the suppression of IX scattering as outlined in the main text and, in turn, require that the disorder in HS is small. It is challenging to manufacture samples with different twist angles, all with sufficiently small disorder, in order to study the dependence of the spin transport on the twist angle and, in turn, on the moiré superlattice period. Consequently, this remains the subject for future works.

Optical measurements

Excitons were generated by a cw Ti:Sapphire laser with the excitation energy $E_{\text{ex}} = 1.689$ eV. PL spectra were measured using a spectrometer with resolution 0.2 meV and a liquid-nitrogen-cooled CCD. The spatial profiles of polarization-resolved IX PL vs. x were obtained from the polarization-resolved PL images detected using the CCD. The signal was integrated from $y = -0.5$ to $y = +0.5 \mu\text{m}$. Figure S2 shows representative polarization-resolved IX PL images.

The IX PL kinetics in the sample was measured in earlier studies [2] using a pulsed semiconductor laser and a liquid-nitrogen-cooled CCD coupled to a PicoStar HR TauTec time-gated intensifier. These measurements showed that the IX lifetimes in the sample are in the range of $\sim 10 - 30$ ns for the densities and temperatures studied in this work and ~ 20 ns for the densities and temperatures corresponding to both the long-distance IX transport and the long-distance spin transport carried by IXs. These measurements also showed that for the densities and temperatures corresponding to both the long-distance IX transport and the long-distance spin transport carried by IXs, the IX propagation is characterized by the average velocity of the IX cloud expansion $v \sim \Delta R / \Delta t \sim 5 \times 10^4$ cm/s. Since the spin transport is carried by IXs, the IX transport kinetics can give a rough estimate for the spin transport kinetics, however, spatially- and polarization-resolved imaging experiments are needed to measure the spin transport kinetics in IXs and this is the subject for future works.

The experiments were performed in a variable-temperature 4He cryostat. The sample was mounted on an Attocube xyz piezo translation stage allowing adjusting the sample position relative to a focusing lens inside the cryostat. All physical phenomena presented in this work are reproducible after ca. 100 cooling down to 2 K and warming up to room temperature.

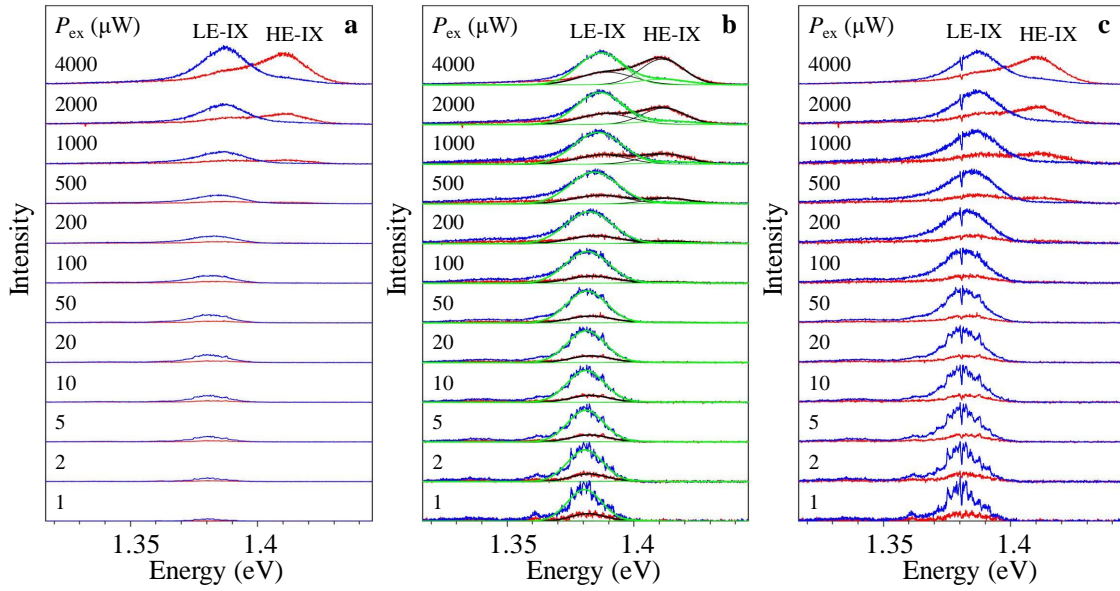


FIG. S3: (a) The excitation power dependence of co-polarized (blue) and cross-polarized (red) IX spectra. The LE-IX PL is co-polarized. The HE-IX PL is cross-polarized. The HE-IXs appear in the spectra at high $P_{\text{ex}} \geq 0.2$ mW. The same spectra with normalized intensities are shown in Fig. 4a. (b) The same spectra as in Fig. 4a with the spectral profile separation of the co-polarized and cross-polarized PL of LE-IXs and HE-IXs. The gaussian fits to the co-polarized (cross-polarized) LE-IX spectra and HE-IX spectra are shown by the thin green (black) lines. The sum of the gaussians shown by the thin green (black) line is shown by the thick green (black) line. (c) The same spectra as in (b) without excluding the part of the spectra affected by the CCD defect at ~ 1.38 eV, which causes an intensity reduction. The parts of the spectra affected by this defect are excluded from the spectra in (b) and other spectra in the paper. $T = 3.5$ K.

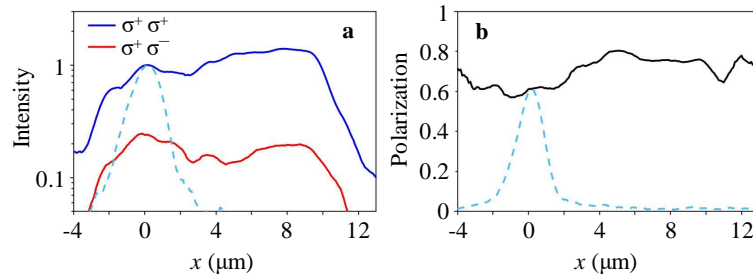


FIG. S4: Same as Fig. 1b,c for LE-IXs with the LE-IX spectra separated from the HE-IX spectra by the gaussian fits. Selecting LE-IXs by the spectral integration in the range $E < 1.4$ eV (as in Fig. 1b,c) or by the spectral integration of the gaussian fits (as in Fig. S4a,b) give similar results.

LE-IX and HE-IX spectral profile separation

We used two methods to separate LE-IX spectra from HE-IXs spectra: (i) by the spectral integration in the range $E < 1.4$ eV where LE-IXs dominate the spectra (Fig. 1a and 4a) and (ii) by the gaussian fits (Fig. S3b). These two methods give similar results: compare Fig. 1b,c with Fig. S4a,b, Fig. 2a-c with Fig. S5a-c, and Fig. 3a-c with Fig. S6a-c where the LE-IX spectra were separated from HE-IX spectra using these two different methods in the two figures in each pair of the figures.

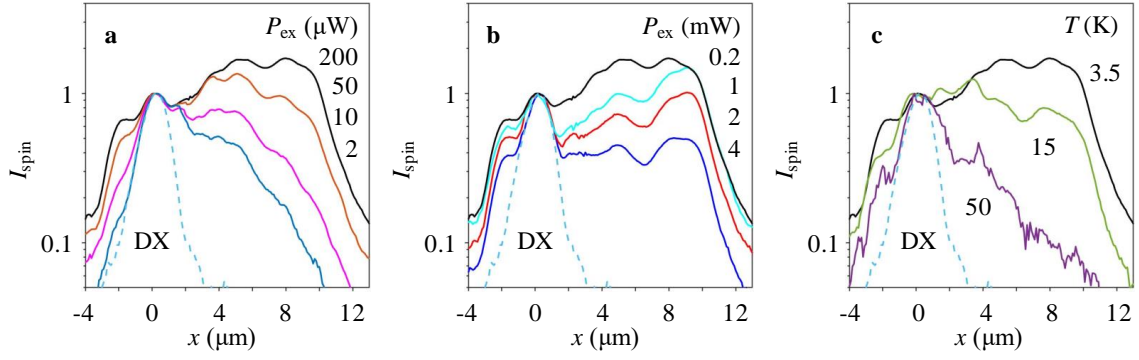


FIG. S5: Same as Fig. 2 for the LE-IXs with the LE-IX spectra separated from the HE-IX spectra by the gaussian fits. Selecting LE-IXs by the spectral integration in the range $E < 1.4$ eV (as in Fig. 2) or by the spectral integration of the gaussian fits (as in Fig. S5) give similar results.

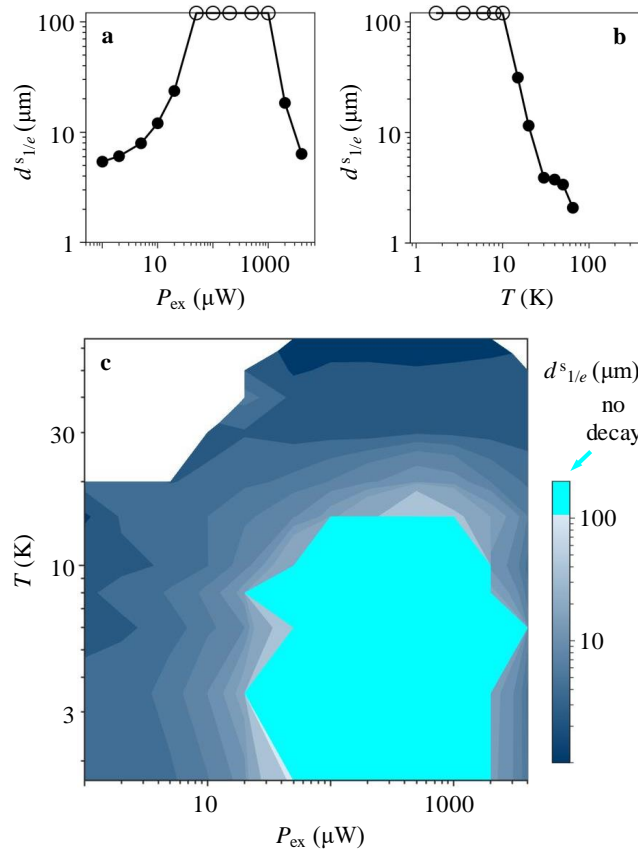


FIG. S6: Same as Fig. 3 for LE-IXs with the LE-IX spectra separated from the HE-IX spectra by the spectral integration in the range $E < 1.4$ eV. Selecting LE-IXs by the spectral integration in the range $E < 1.4$ eV (as in Fig. S6) or by the spectral integration of the gaussian fits (as in Fig. 3) give similar results.

The density and temperature dependence of LE-IX transport

The LE-IX transport is characterized by the $1/e$ decay distance $d_{1/e}$ of the LE-IX PL intensity $I = I_{\sigma^+} + I_{\sigma^-}$ (Fig. S7 and S8). In these two figures LE-IX spectra are separated from HE-IX spectra using the two methods outlined above. Figures S7 and S8 show that these two methods give similar results.

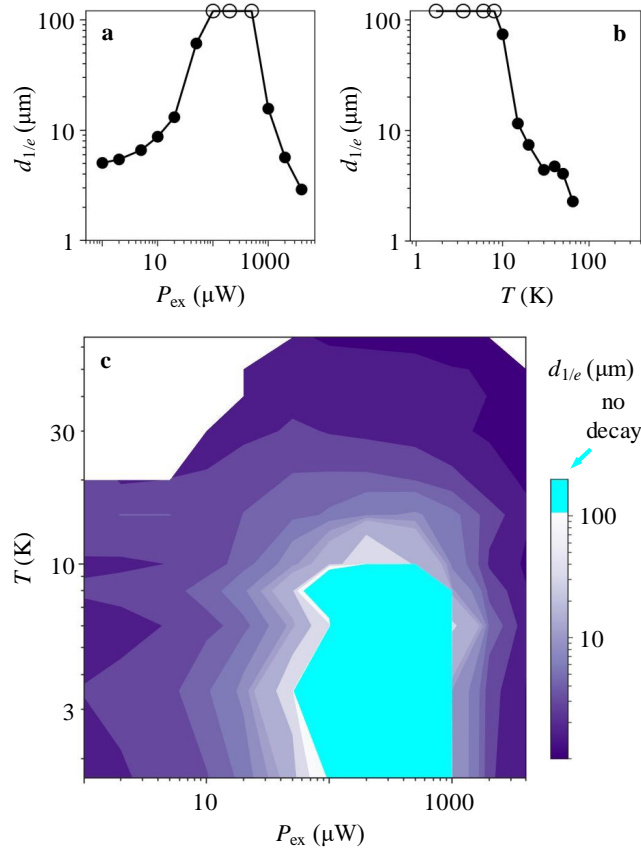


FIG. S7: Excitation power and temperature dependence of LE-IX transport. (a,b) The $1/e$ decay distance $d_{1/e}$ of LE-IX PL intensity $I = I_{\sigma^+} + I_{\sigma^-}$ vs. P_{ex} (a), vs. temperature (b), and vs. P_{ex} and temperature (c). $d_{1/e}$ are obtained from least-squares fitting the LE-IX intensity profiles $I(x)$ to exponential decays in the region $x = 0 - 9 \mu\text{m}$. The data with the fit indicating diverging $d_{1/e}$ are presented by circles on the edge (a,b) or by cyan color (c). The LE-IX spectra are separated from the HE-IX spectra by the spectral integration of the gaussian fits. $T = 3.5 \text{ K}$ (a), $P_{\text{ex}} = 0.2 \text{ mW}$ (b).

The density and temperature dependence of LE-IX transport (Figs. S7 and S8) is qualitatively similar to the density and temperature dependence of IX transport [2]. The latter refers to transport of all IXs, including LE-IXs and HE-IXs, and has a narrower $d_{1/e}(P_{\text{ex}})$ profile, in particular, because HE-IXs have shorter transport distances. The density and temperature dependence of spin transport in LE-IXs (Fig. 3) is qualitatively similar to the density and temperature dependence of LE-IX transport (Figs. S7 and S8) as outlined in the main text.

The LE-IX intensity enhancement with density slows at intermediate densities (Fig. 4b). This is qualitatively consistent with a more effective LE-IX cloud expansion from the excitation spot due to the longer-distance LE-IX transport at these densities (Figs. S7 and S8).

The temperature dependence of co-polarized and cross-polarized IX PL

The temperature dependence of co-polarized and cross-polarized IX spectra is presented in Fig. S9. The temperature increase causes a reduction of the degree of circular polarization of LE-IX PL $P = (I_{\sigma^+} - I_{\sigma^-}) / (I_{\sigma^+} + I_{\sigma^-})$ (Fig. S9c). However, this reduction is rather small, with no sharp changes at $T \sim 10 \text{ K}$ where the transport of spin polarization density I_{spin} carried by LE-IX sharply drops (Fig. 3). This confirms that the dominant mechanism of the decay of spin density $I_{\text{spin}} = Pn$ is the decay of IX density as outlined in the main text.

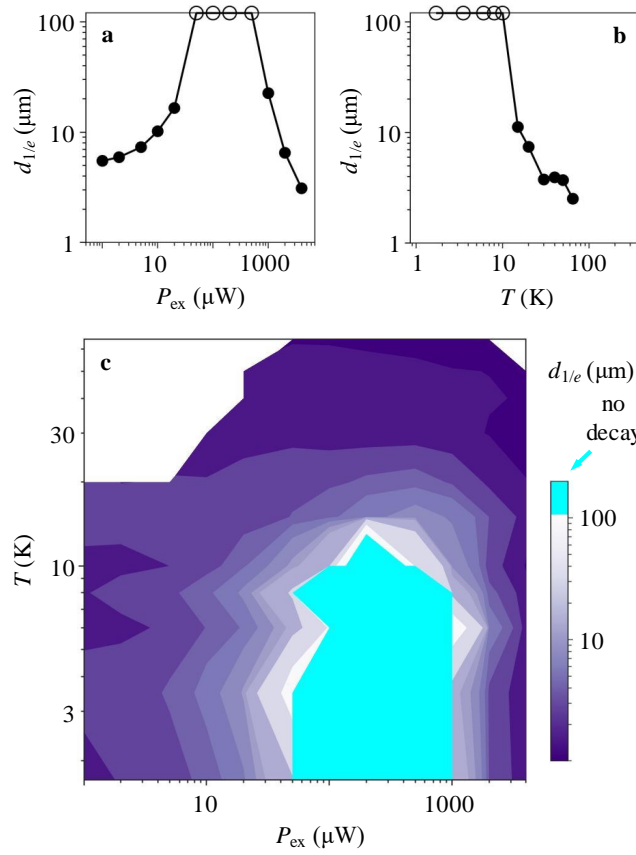


FIG. S8: Same as Fig. S7 for LE-IXs with the LE-IX spectra separated from the HE-IX spectra by the spectral integration in the range $E < 1.4 \text{ eV}$. Selecting LE-IXs by the spectral integration in the range $E < 1.4 \text{ eV}$ (as in Fig. S8) or by the spectral integration of the gaussian fits (as in Fig. S7) give similar results.

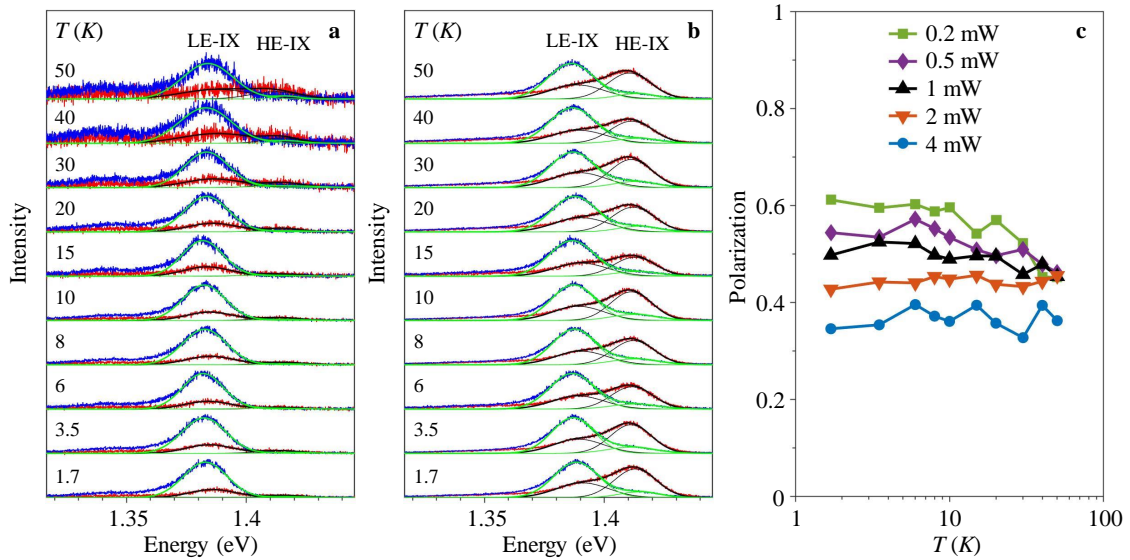


FIG. S9: (a,b) The temperature dependence of co-polarized (blue) and cross-polarized (red) IX spectra at $P_{\text{ex}} = 0.2 \text{ mW}$ (a) and 4 mW (b). The LE-IX PL is co-polarized. The HE-IX PL is cross-polarized. The HE-IXs appear in the spectra at high $P_{\text{ex}} \gtrsim 0.2 \text{ mW}$. The intensities are normalized. (c) The degree of circular polarization of LE-IX PL $P = (I_{\sigma^+} - I_{\sigma^-}) / (I_{\sigma^+} + I_{\sigma^-})$ vs. temperature at different P_{ex} . The LE-IX spectra are separated from the HE-IX spectra by the gaussian fits.

-
- [1] F. Withers, O. Del Pozo-Zamudio, A. Mishchenko, A.P. Rooney, A. Gholinia, K. Watanabe, T. Taniguchi, S.J. Haigh, A.K. Geim, A.I. Tartakovskii, K.S. Novoselov, Light-emitting diodes by band-structure engineering in van der Waals heterostructures. *Nat. Mater.* **14**, 301 (2015).
 - [2] L.H. Fowler-Gerace, Zhiwen Zhou, E.A. Szwed, D.J. Choksy, L.V. Butov, Transport and localization of indirect excitons in a van der Waals heterostructure. arXiv:2307.00702 (2023).
 - [3] Fengcheng Wu, Timothy Lovorn, A.H. MacDonald, Theory of optical absorption by interlayer excitons in transition metal dichalcogenide heterobilayers. *Phys. Rev. B* **97**, 035306 (2018).
 - [4] Hongyi Yu, Gui-Bin Liu, Wang Yao, Brightened spin-triplet interlayer excitons and optical selection rules in van der Waals heterobilayers. *2D Mater.* **5**, 035021 (2018).
 - [5] Fengcheng Wu, Timothy Lovorn, A.H. MacDonald, Topological Exciton Bands in Moiré Heterojunctions. *Phys. Rev. Lett.* **118**, 147401 (2017).
 - [6] Hongyi Yu, Gui-Bin Liu, Jianju Tang, Xiaodong Xu, Wang Yao, Moiré excitons: From programmable quantum emitter arrays to spin-orbit-coupled artificial lattices. *Sci. Adv.* **3**, e1701696 (2017).